

# Geologic lithofacies identification using the multiscale character of seismic reflections

Moshe Strauss and Micha Sapir  
*Nuclear Research Center, Negev, Beer Sheva, Israel*

Michael E. Glinsky<sup>a)</sup> and Jesse J. Melick  
*BHP Billiton Petroleum, Houston, Texas 77056-3020*

(Received 27 January 2003; accepted 28 July 2003)

A forward acoustic model shows that geologic lithofacies groups can be identified by the character of the wavelet transform of their seismic reflection response even for incident signals with a wavelength much larger than the dominant bed thickness. The same model shows that multiple interbed reflections can be neglected. This allows the use of an analytical relation of the linear reflection response expressed as a convolution between the incident signal and the scaled derivative of the acoustic impedance. The relation is applied to solve the inverse problem for the acoustic impedance, using orthogonal discrete wavelet transform (DWT) and Fourier transform methods; good agreement is obtained between the well log wavelet spectrum and both the forward modeled seismic data and the real seismic data. It is found that the DWT approach is superior, having a better signal-to-noise ratio and more localized deconvolution artifacts. A population of well logs containing a wide range of lithologies and bed thicknesses, which are categorized into lithofacies groups, is used to define the conditional probability of a wavelet transform response given a lithofacies group. These conditional probabilities are used to estimate the lithofacies probability given a seismic wavelet response via a Bayesian inversion. © 2003 American Institute of Physics. [DOI: 10.1063/1.1610241]

## I. INTRODUCTION

The multiscale character of geologic sedimentation and how it manifests itself in the seismic reflection record has been studied by many authors. This has ranged from examining the frequency distribution of beds,<sup>1-3</sup> to examining the theoretic reflection response of statistically generated bed sequences,<sup>4</sup> to statistical correlation of hyperspectral seismic attributes,<sup>5</sup> and log response using neural networks.

There has also been a recent body of research that has appeared in the image processing and target recognition literature that has used wavelet-based techniques to analyze transient signals.<sup>6</sup> It has also been recognized that wavelet analysis is the best and most fundamental way to analyze a multiscale signal.<sup>7-9</sup>

This article recognizes the multiscale character of depositional sequences that has been examined by many authors, and the efficacy of wavelet decompositions in analyzing multiscale signals. It establishes the fundamental relationship between the wavelet decomposition of the acoustic properties of the rock sequences and the wavelet decomposition of the seismic reflection response. This relationship is inverted so that the wavelet decomposition of the rocks can be determined from the wavelet decomposition of the seismic reflection response. It is found that even very low frequency seismic data (10 Hz) can distinguish rock packages that have a dominant bed thickness that would require frequencies greater than 60 Hz to resolve. A population of well logs is analyzed to determine the characteristics of their wavelet

transformations given the vertical distribution of their gross lithologies and bed thicknesses, or lithofacies. The inverse relationship along with the knowledge of the multiscale character of stratigraphy, allows one to analytically determine the probability of a lithofacies given low frequency seismic data.

An important consideration is the impact of noise on the inversion of the seismic reflection response and the ability to identify the lithofacies. Coherent noise is very prominent on real seismic data. This noise must be taken into account in the inversion or it will be unstable and the results unreliable. Significant steps are taken in the inversion to deal with this. There is an imbedded assumption of randomness in these methods. Since noise in real seismic data has a significant coherent component, the inversion algorithms were applied to the real seismic data to see how well the wavelet spectrum of the rocks could be recovered. A very good result is found.

The difference between this and previous methods lies in its rational, model-based approach. Attempts at statistical correlation, that is assay, of seismic response to underlying geology suffer from (1) limited data where both a well log and good seismic exist, (2) biased data where high net pay sands are preferentially sampled, and (3) an inability to extrapolate beyond the range of sampled physical situations. A rational, model-based approach allows well logs to be used where there are no reliable seismic data, a compensation to be made for the biased sampling, and a reliable extrapolation to be made due to the constraints of the model.

The potential business value lies in the determination of the probability of the lithofacies. Each lithofacies can be characterized in terms of the range of its volumetric proper-

<sup>a)</sup>Electronic mail: michael.e.glinsky@bhpbilliton.com

ties such as net sandstone percent and sandstone packaging thickness, and reservoir flow properties such as the ratio between the vertical and horizontal permeabilities. A more definitive determination of the probability of the lithofacies will reduce the uncertainty in the recoverable volumes, well count, and production rates. This will allow better business decisions to be made, creating fiscal value.

This article presents, in Sec. II, how the continuous wavelet transform (CWT) can be used to distinguish the differences in the acoustic properties of two end member lithofacies. An analytic estimate is made, in Sec. III, of the seismic reflection response by forward modeling using a hydrodynamic, that is acoustic, computer algorithm that does not allow for shear wave propagation.<sup>10,11</sup> An extension of this modeling shows that multiple interbedded reflections are not important. This allows a linear approximation to be made, in Sec. IV, and a relationship inverted to give the wavelet decomposition of the lithofacies given the wavelet decomposition of the seismic reflection response. It is shown that the discrete wavelet transform<sup>12,13</sup> (DWT) gives a superior inversion compared to the Fourier transform (FT). In Sec. V, the inversion relationship is applied to the real seismic data corresponding to the two modeled rock lithofacies. Very good agreement is found. In Sec. VI, the conditional probability of a CWT given a lithofacies is determined from well logs, and the probability of a lithofacies given a seismic wavelet transform response is calculated for the two real seismic data examples.

## II. WAVELET DECOMPOSITION OF ACOUSTIC ROCK PROPERTIES

Two geologic lithofacies groups are the testbed for this analysis. They have significantly different depositional environments and different bed sequencing, that is different multiscale behavior. They will be called lithofacies A and B. A well database of 11 cases for lithofacies A and 15 cases for lithofacies B were used in this study. One characteristic case was used from each group for the more detailed analysis. Although many of the cases did not have good seismic which corresponded to the well log data, both characteristic cases did have good seismic data, even though the seismic data had significant differences in acquisition, processing, and the wavelet. An approximate 250 m segment was clipped out of the well logs (density,  $\rho$ , and sound speed,  $c$ ) for the two characteristic cases. A 100 m cosine taper was used to mitigate the effect of the clipping. The clipping points were also chosen in a zone of relatively weak reflectivity to also mitigate the clipping effect. It was verified that the clipping made little difference to the wavelet decomposition in the zone of interest. The derivative of the acoustic impedance  $\rho c$  is shown as a function of depth for both characteristic cases in Fig. 1. There is little difference between the appearance of these two signals. There are two bed sizes shown as bars in Fig. 1(a). These will be discussed in a moment.

The CWT is then taken of the two signals to highlight the differences between lithofacies A and B. The CWT is applied to a signal  $\psi(x)$  by a convolution

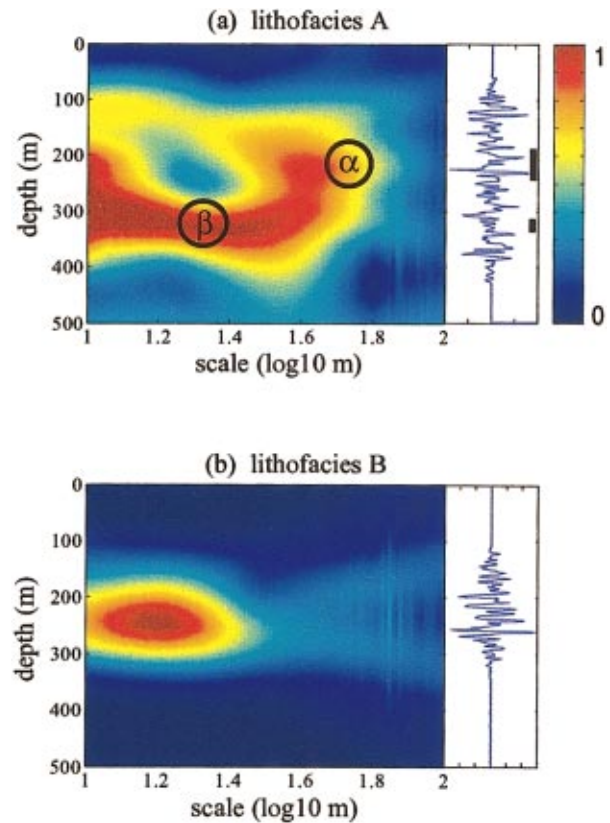


FIG. 1. (Color) Derivative of the well log acoustic impedance vs depth shown as the blue line graph on the right, continuous wavelet transform (CWT) plotted as the color image. The CWT has had a 30 m boxcar smoother applied in the depth direction to its absolute value. The color bar is shown on the right-hand side. It ranges from 0 to the maximum value of the CWT normalized to 1. This will be true of all CWTs that are displayed in the figures. (a) Lithofacies A, the part of the CWT shown as the  $\alpha$  circle corresponds to beds of the size and location of the larger bar shown on the blue line graph, the  $\beta$  circle corresponds to the smaller bar. (b) Lithofacies B.

$$\hat{\psi}_\sigma(x) = \int_0^\infty dx' \psi(x') u_\sigma(x' - x), \quad (1)$$

where  $u_\sigma(x)$  is a set of basis functions of scale  $\sigma$ . The basis used is the Mexican hat basis

$$u_\sigma(x) = [1 - (2x^2/\sigma^2)] \exp(-x^2/\sigma^2), \quad (2)$$

chosen because of its similarity to the incident wavelet of typical seismic data. Once this CWT is applied to the signal the absolute value is taken and then it is smoothed by a boxcar filter of length 30 m in the  $x$  direction. This smoothing is done to match the typical depth resolution of seismic data. If this smoothing is not done, it is very difficult to compare the response to that of the seismic data—there is just too much detail in the well log data. The CWT of the two signals are shown in Fig. 1. The CWT is shown as a colored image in depth,  $x$  and scale,  $\sigma$ , where the color is determined by the smoothed absolute magnitude of the CWT. Note the significant differences between the two lithofacies. Lithofacies A shows a complex structure of beds of size 50 m near the top of the package [note the circle labeled  $\alpha$  in Fig. 1(a), and the large bar in Fig. 1(a)], and beds of many sizes including 20 m [note the circle labeled  $\beta$  in Fig.

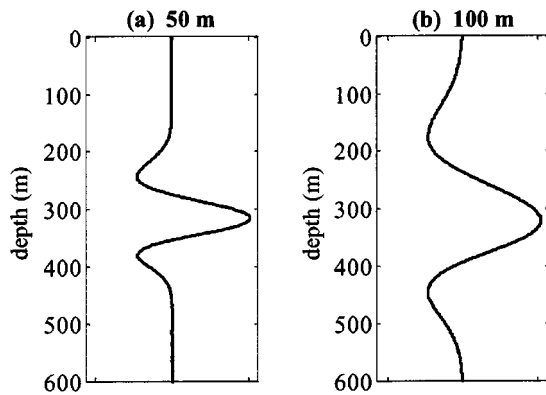


FIG. 2. Incident Mexican hat wavelets shown as amplitude (arbitrary units) vs depth for (a)  $\sigma=50$  m and (b)  $\sigma=100$  m.

1(a), and the small bar in Fig. 1(a)] near the bottom of the package. Lithofacies B, in Fig. 1(b), has a much simpler structure with a single dominant bed size of 15 m. The question now is whether these differences can be seen in the seismic data. For reference, the seismic frequency of a reflection off of a 10 m bed is about 100 Hz, and off of a 100 m bed is about 10 Hz.

### III. FORWARD MODELING OF REFLECTION RESPONSE

#### A. Acoustic model

The seismic expression of the two distinct lithofacies is examined using a hydrodynamic, finite difference, computer model.<sup>10,11</sup> The model allows only compressional, that is, acoustic waves. It is valid for all internal reflections and accounts for full wave propagation and strong reflections. Since the simulation is one-dimensional, angle-dependent reflections are ignored. The use of this model is to justify the approximation of the linear reflection.

The signal is propagated by the model through the well log profiles of density and compressional sound speed, which are sampled at 1 m intervals (subsampling from a resolution of 0.33 m after a boxcar filter of 1 m is applied). It is verified that the subsampling makes no significant difference to the results.

The medium is represented by a Gruneisen equation of state<sup>14,15</sup> (EOS) valid for the range of pressures in seismic imaging. The EOS is a simple analytical relationship between the density, pressure, temperature, and energy. It depends on a small number of parameters—the initial local density; the initial sound speed; the dimensionless Gruneisen factor  $\gamma$ , which connects the pressure and the energy; and the dimensionless factor  $S$ , which includes the particle velocity contribution to the sound speed. For typical rocks  $\gamma \approx 1$  and  $S \approx 1.5$ . For the seismic range of small acoustic pressures, the signal propagation is independent of the detailed value of these parameters.

The simulation is initialized so that there is an incident pressure pulse in the form of a Mexican hat wavelet,  $\psi_\sigma(x)$ , where  $\sigma$  is the scale and the functional form is given by Eq. (2). Simulations are done for two different scales for the incident wavelet, 50 and 100 m, which correspond to fre-

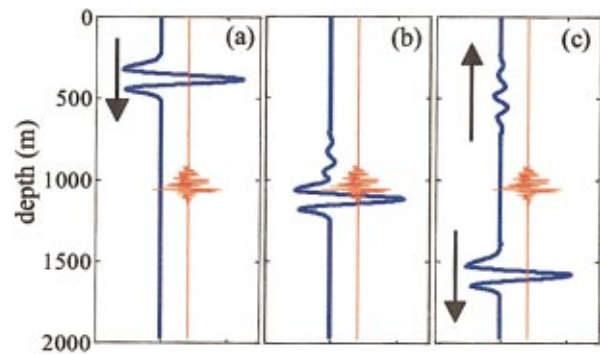


FIG. 3. (Color) Pressure profile (thick blue line) and the derivative of the acoustic impedance profile (thin red line) shown in arbitrary units vs depth for a time (a) before, (b) during, and (c) after the reflection. The arrows indicate the direction of propagation of the pressure pulse. The profiles are for lithofacies B and the incident pressure profile is the same as shown in Fig. 2(a).

quencies of 20 and 10 Hz, respectively (see Fig. 2). In Fig. 3(a), the incident pressure pulse is shown along with the derivative of the acoustic impedance for lithofacies B (wavelet scale 50 m). The pressure pulse during the interaction is shown in Fig. 3(b), and the reflected and transmitted pulses are displayed in Fig. 3(c).

The CWTs of the reflected signals (with the depth scale divided by 2, accounting for the two-way travel time of the reflection) are shown in Figs. 4 and 5. Note the significant differences between the two lithofacies for both the 10 and

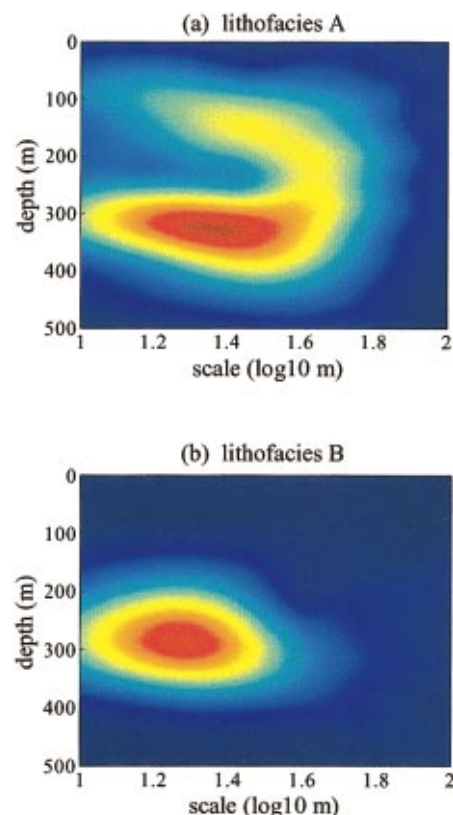


FIG. 4. (Color) CWT of the hydrodynamically (acoustically) simulated seismic reflection for an incident 50 m Mexican hat wavelet. (a) Lithofacies A. (b) Lithofacies B.

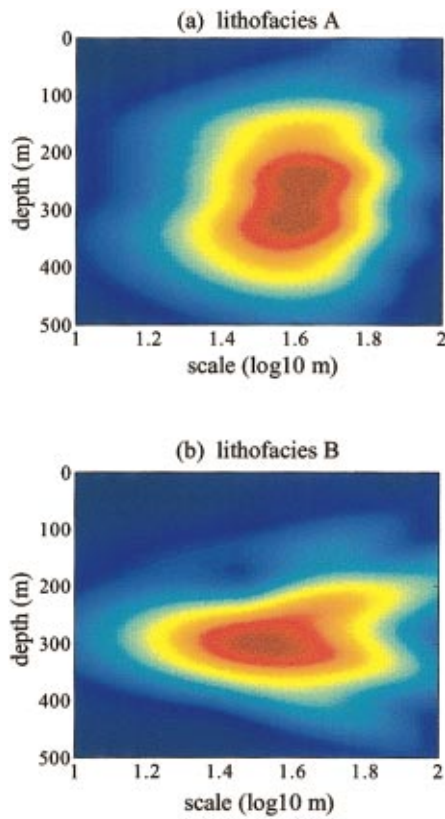


FIG. 5. (Color) CWT of the hydrodynamically (acoustically) simulated seismic reflection for an incident 100 m Mexican hat wavelet. (a) Lithofacies A. (b) Lithofacies B.

20 Hz incident signals. The central frequency for Fig. 1(b) is close to 60 Hz yet there are significant differences between Figs. 4(a) and 4(b), and even between Figs. 5(a) and 5(b). The problem is that the characteristics of the CWT of the reflected signal are dependent on the incident wavelet. A procedure needs to be derived to reduce this dependency. A key enabler for this will be linearization of the seismic reflection—multiple reflections will need to be neglected.

**B. Contribution of multiple reflections**

The hydrodynamic model is modified to have a parameter that amplifies or attenuates the effects of multiple reflections (MRs). This is based on changing the impedance difference (local reflectivity) between very close hydrodynamic zones by a constant factor  $f_{imp}$ . The change in the impedances obtained by very small virtual shifts of the initial density in every hydrodynamic zone. For example, in zone  $i$  with initial density  $\rho_{0,i}$ , the density is changed to  $\rho_i$  using the local reflection relation,

$$\frac{c_i \rho_i - c_{i-1} \rho_{i-1}}{c_i \rho_i + c_{i-1} \rho_{i-1}} = f_{imp} \frac{c_i \rho_{0,i} - c_{i-1} \rho_{0,i-1}}{c_i \rho_{0,i} + c_{i-1} \rho_{0,i-1}}, \quad (3)$$

where the local sound speed  $c_i$  is unchanged. Using Eq. (3),  $\rho_i$  can be expressed in terms of  $\rho_{0,i}$ ,  $f_{imp}$ , and  $\rho_{i-1}$ , where we start from  $i = 1$  and  $\rho_1 = \rho_{0,1}$ . The first-order contribution to the reflected signal is changed by a factor  $f_{imp}$ , but the higher order MR contributions differ by additional factors of  $f_{imp}^2$ . Selecting  $f_{imp}^2 \ll 1$  can arbitrarily reduce the MR terms.

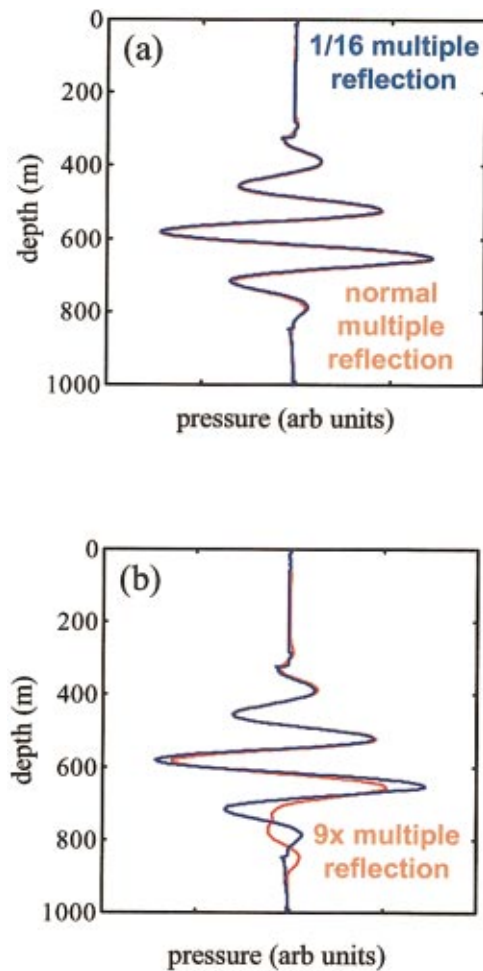


FIG. 6. (Color) Reflected pressure pulse vs depth for (a)  $f_{imp}^2 = 1$  in red and  $f_{imp}^2 = 1/16$  in blue, and (b)  $f_{imp}^2 = 9$  in red and  $f_{imp}^2 = 1/16$  in blue. Profiles are for lithofacies B.

Selecting  $f_{imp}^2 > 1$ , increases the relative MR contribution. By setting  $f_{imp}^2 \ll 1$  (excluding the MR terms), then restoring the reflected signal by multiplying the reflected signal by  $1/f_{imp}$  one gets only the first-order reflection. The amount of multiple reflection can now be found by comparing the case with  $f_{imp} = 1$  (with MR) to the case  $f_{imp}^2 \ll 1$  (without MR). By setting  $f_{imp} > 1$  we can study the effect of amplified MR.

Figure 6(a) shows the amount of multiple reflection. It compares the case with  $f_{imp} = 1/4$  (with a reduction in the multiple reflection by  $f_{imp}^2 = 1/16$ ) to the case with  $f_{imp} = 1$ . No significant difference is seen (2.4% of the energy, and no significant change in the shape of the wavelet transform). The effect of MR is amplified in Fig. 6(b). MR is increased by a factor of  $f_{imp}^2 = 9$ . It is compared to the case with very little multiple reflections,  $f_{imp}^2 = 1/16$ . Note the significant modification to the trailing end of the pulse due to the interbed reflections. The leading edge of the pulse has little modification due to the interbed reflections. Therefore, even for a case with moderate amounts of multiple reflections, the leading edge of a package of reflections can be predicted by using only the first-order, linear, reflections.

**IV. INVERSE MODEL**

**A. Analytical expression for reflection response**

A linear scattering approximation is made since the effect of multiple reflections can be neglected for the cases being considered. This allows the reflection response to be written as a convolution between the incident signal and the derivative of the acoustic impedance. A change of scale for the acoustic impedance is necessary to account for the two-way travel time.

The acoustic impedance is divided into small intervals  $dx$ . Express the reflection response  $R(x)$  in terms of the incident signal  $\psi(x)$  and the acoustic impedance jump  $dg_{ac}(x)$  in the intervals  $dx$ ,

$$R(x) = \int_{-\infty}^{\infty} \frac{dg_{ac}(x')}{g_{ac}(x')} \frac{c_0}{c(x')} \psi(x' - x), \tag{4}$$

where  $g_{ac}(x)$  in the impedance and its spatial dimension is scaled by a factor of 2, so that  $x \rightarrow 2x$ . This scaling is a time delay due to the fact that the input signal and the reflected signal travel the interval  $dx$  twice. In Eq. (4) include the rescaling of the interval  $dx'$  by the local change in the sound speed,  $dx' \rightarrow dx' c_0/c(x')$ , where  $c(x')$  and  $c_0$  are the local and the average acoustic sound speed in the reflection range, respectively. Assume in Eq. (4) that the variation in sound speed and in the acoustic impedance is small, consistent with the linear approximation

$$R(x) = \frac{1}{g_0} \int_{-\infty}^{\infty} \psi(x' - x) g'_{ac}(x') dx', \tag{5}$$

where  $dg_{ac} = g'_{ac} \cdot dx$ ,  $g'_{ac}$  is the impedance derivative, and  $g_0$  is the average impedance in the reflected range. Assuming that the incoming function is a wavelet  $\psi_{\sigma}(x)$  with scale length  $\sigma$  obtain,

$$R(x) = \frac{1}{g_0} \int_{-\infty}^{\infty} g'_{ac}(x') \psi_{\sigma}(x' - x) dx'. \tag{6}$$

In Eq. (6) the reflection function is expressed as a wavelet transform of the scaled impedance derivative.

To test the validity of the analytical relation, Eq. (6), its prediction of the reflection response is compared to the hydrodynamic result of Sec. III, which includes all the effects ignored in the analytic treatment. When this is done, no significant difference is found. This is further confirmation that the linear approximation is justified.

**B. Discrete wavelet transform inverse model**

In this section, deconvolution methods (using an orthonormal discrete wavelet transform method) are applied to solve the inverse problem. Starting with Eq. (6), which expresses the reflection  $R(x)$  as a convolution between the impedance derivative  $g'_{ac}(x)$  and the incoming signal  $\psi_{\sigma}(x)$ , an orthogonal wavelet basis is used to invert Eq. (6) and obtain the impedance  $g_{ac}(x)$  as a function of the reflection  $R(x)$ .

The wavelet basis functions  $u_{jn}(x)$  are

$$u_{jn}(x) = \frac{1}{\sqrt{2^j}} u\left(\frac{x - 2^j n}{2^j}\right), \tag{7}$$

where  $u_{jn}(x)$  is the basic wavelet (scaled by  $2^j$  and shifted by  $2^j n$ ),  $j$  is the scale level, and  $n$  the shift number. They satisfy orthogonality and completeness relations. The wavelet transform of a function,  $f(x)$ , is defined as

$$\hat{f}_{jn} = \int_{-\infty}^{\infty} u_{jn}(x') f(x') dx'. \tag{8}$$

Start with the expansions,

$$g'_{ac}(x) = \sum_{jn} a_{jn} u_{jn}(x), \tag{9}$$

and

$$R(x) = \sum_{jn} b_{jn} u_{jn}(x), \tag{10}$$

where integration of Eq. (9) over  $x$  yields an explicit expression for the scaled,  $x \rightarrow 2x$ , impedance  $g_{ac}(x)$ . Apply the orthogonal relation to calculate  $b_{jn}$  as a wavelet transform,

$$b_{jn} = \int_{-\infty}^{\infty} R(x') u_{jn}^*(x') dx'. \tag{11}$$

The relation between  $a_{jn}$  and  $b_{jn}$  can be written as

$$b_{jn} = \sum_{j'n'} M_{jn,j'n'} a_{j'n'}, \tag{12}$$

then inverted to give

$$a_{jn} = \sum_{j'n'} M_{jn,j'n'}^{-1} b_{j'n'}. \tag{13}$$

The coupling matrix  $M$  is

$$M_{jn,j'n'} = \int_{-\infty}^{\infty} dx u_{jn}^*(x) \int_{-\infty}^{\infty} dx' u_{j'n'}(x') \psi_{\sigma}(x' - x). \tag{14}$$

Write the matrix  $M$  as a double wavelet transform. The first transform is

$$\hat{\psi}_{j'n'}(x) = \int_{-\infty}^{\infty} dx' u_{j'n'}(x') \psi_{\sigma}(x' - x), \tag{15}$$

where  $x$  appears as a parameter that shifts the incoming signal along the spatial axis. The second transform expresses  $M$  as a wavelet transform of  $\hat{\psi}_{j'n'}(x)$ ,

$$M_{jn,j'n'}(x) = \int_{-\infty}^{\infty} dx u_{jn}^*(x) \hat{\psi}_{j'n'}(x). \tag{16}$$

Calculate  $b_{jn}$  by using Eq. (11) and invert the matrix  $M$  given by Eqs. (15) and (16). Insert the results into Eq. (13), to get the impedance coefficient  $a_{jn}$ . Putting these  $a_{jn}$  into Eq. (9), then integrating over  $x$  gives the inverse solution for the scaled,  $x \rightarrow 2x$ , impedance  $g_{ac}(x)$ .

In order to have the most compact representation of the signal in the wavelet transform space, the third-order coiflets are chosen.<sup>16</sup> They are an orthonormal family of wavelets in a finite interval  $L = 2^{j_0}$ , where  $j_0$  is an integer. As shown in Fig. 7, they closely resemble a typical seismic wavelet.

The expansion of a given signal requires the inclusion of wavelet states that extend out of the spatial range  $L$ . These

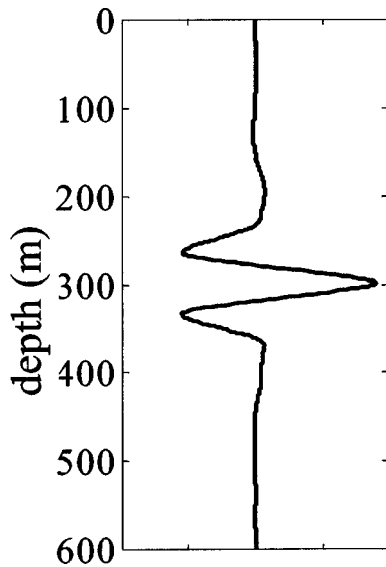


FIG. 7. Third-order coiflet of scale level  $j=6$  shown as amplitude (arbitrary units) vs depth.

states are called boundary states. Define the norm  $N_{jn}$  of states  $u_{jn}(x)$  by the amount of the wavelet in the range  $L$ ,

$$N_{jn} = \int_0^L u_{jn}(x') u_{jn}^*(x') dx'. \tag{17}$$

States with  $N_{jn} \approx 1$  are almost completely in the range  $L$  and are nearly orthogonal states. States  $N_{jn} \ll 1$  are almost excluded from range  $L$ . Boundary states can be included in the expansion if the part of the wavelet out of the spatial range  $L$  has a small overlap with the signals. Many states with small norms have a small overlap with the incoming and reflected signals and do not contribute to the impedance convergence. For decomposition of a signal using a reduced wavelet set, only include boundary states with norm,  $N_{jn}$ , larger than a selected value  $N_0$ , where the value of  $N_0$  depends on the range  $L$ . The smaller  $L$  is, the more boundary states need to be included. Typically,  $N_0 \approx 0.5-0.8$ . For large  $L$  few boundary states need to be included, leaving nearly orthogonal states with  $N_0 \approx 1$ . Reduction of  $N_0$  by a factor of 2 has little effect on the convergence, but more dramatic reductions in  $N_0$  may cause too many boundary states with small norms to be included and convergence is affected.

For the two characteristic lithofacies,  $L=1024$  and  $2048$  m are considered. To obtain convergence of the impedance in an interval  $L=1024$  m boundary states with norm greater than  $N_0 \approx 0.8$  must be included. Selecting  $L=2048$  m allows a more restricted set with a norm greater than  $N_0 \approx 0.99$ , which is almost orthogonal in the interval  $L$ .

The largest scale level  $j_{\max}$  with scale  $2^{j_{\max}}$  needed is  $(\log L/\log 2)-1$ . If  $L=1024$  or  $2048$  m, then  $j_{\max}=9$  or  $10$ , respectively. For an incoming wavelet with scale length,  $\sigma=50$  m, one will need to retain scales with scales greater than or equal to  $j_{\min}=6$ . So the scale length levels included in the inversion are  $j_{\min} \leq j \leq j_{\max}$ . Increasing or decreasing the scale length,  $\sigma$ , of the incoming signal requires an increase or reduction in the lower level  $j_{\min}$ , respectively.

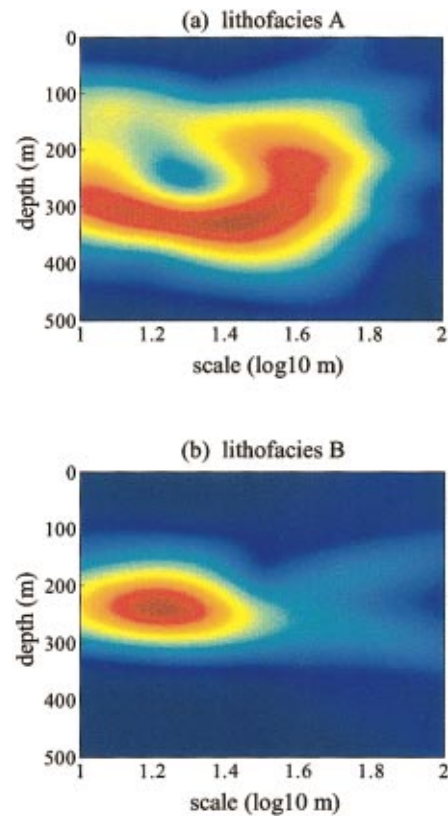


FIG. 8. (Color) CWT of the DWT inversion of the simulated seismic reflection for an incident 50 m Mexican hat wavelet. (a) Lithofacies A. (b) Lithofacies B.

The wavelet transform is taken of the incoming and reflected signals. The coefficients are reduced to the ones which are within the range  $j_{\min} \leq j \leq j_{\max}$ , and have  $N_{jn} > N_0$ . The inverse wavelet transform is then taken and compared to original signals to check that there is reasonable agreement. This verifies that the reduction in the coefficients will not affect the inversion result. The decomposition of the reflected signal gives the coefficients  $b_{jn}$  of Eq. (11). For both  $L=1024$  or  $2048$  m, the number of reduced states is close to 45.

Obtain the matrix  $M$  by numerically applying the double wavelet transform given by Eqs. (15) and (16). The matrix  $M$  is reduced by using only the coefficients used for  $b_{jn}$ . Inverting the reduced  $M$  matrix to get  $M^{-1}$ , then substituting the result into Eq. (13) along with the coefficients  $b_{jn}$  derived from the decomposition of the reflected signal gives the coefficients  $a_{jn}$ . Using Eq. (9), and integrating over  $x$ , leads to the inverse solution for the impedance  $g_{ac}(x)$ .

This DWT inversion is applied to the acoustic simulation of the seismic reflection off the two lithofacies. The CWT is then taken of the inverted signal. The results for the simulation using the 50 m (20 Hz) incident wavelet are shown Fig. 8, and for the simulation using the 100 m (10 Hz) incident wavelet are shown in Fig. 9. Note the similarity of both figures to Fig. 1, the CWT of the well log data. There is a small attenuation in Fig. 8 of the 20 Hz CWT at the smallest scale when compared to the well log CWT in Fig. 1. This is caused by the finite bandwidth of the 20 Hz data. There was

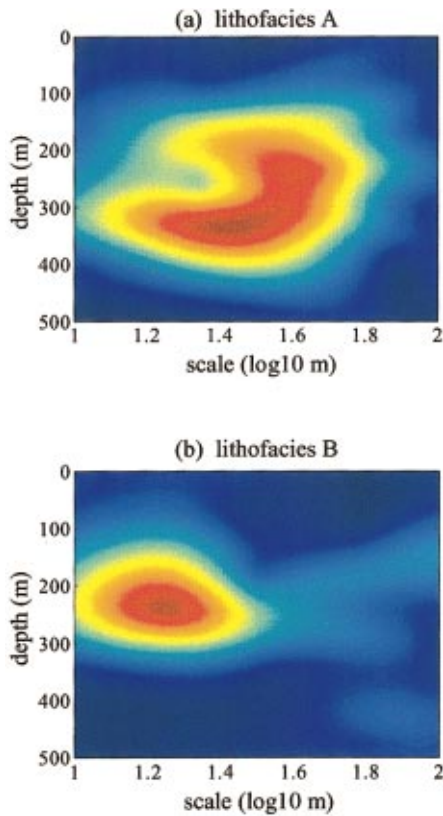


FIG. 9. (Color) CWT of the DWT inversion of the simulated seismic reflection for an incident 100 m Mexican hat wavelet. (a) Lithofacies A. (b) Lithofacies B.

not enough reflected energy of these small scales. The inversion could not restore these scales without amplifying noise. This attenuation, in Fig. 9, extends to slightly larger scales in the CWT of the 10 Hz data. There is a significant improvement when the inverted CWTs are compared to the CWTs of the reflected signal shown in Figs. 4 and 5. There is much less imprint of the incident wavelet. Where there is significant energy in the inverted CWTs, it has the same pattern as the CWT of the well log data. Since each seismic data set will have a different wavelet and the same dataset may even have a different wavelet for different depths due to inelastic attenuation, this inversion process will allow a normalization of the CWT of the reflected signals so that they can be compared to the well log calibration database.

### C. Fourier transform inverse model

Although the DWT inversion (deconvolution) works well, there is obviously the more common Fourier transform method for accomplishing the same task. This section will outline this method and show that the performance of the DWT method is superior.

Taking the Fourier transform in Eq. (5),

$$\hat{g}'_{ac}(k) = \hat{R}(k) / \hat{\psi}_{\sigma}(k), \quad (18)$$

the inverse Fourier transform of Eq. (18) gives the impedance derivative

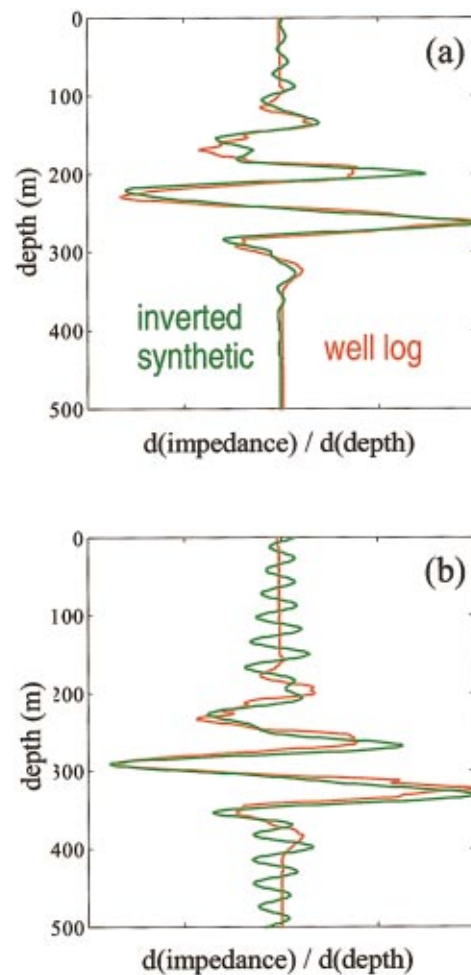


FIG. 10. (Color) Smoothed (30 m boxcar) derivative of the acoustic impedance in arbitrary units vs depth (red) compared to the inverted simulated seismic reflection (green) for (a) DWT inversion method ( $S/N=22.1$  dB), and (b) FT inversion method ( $S/N=13.8$  dB). Profiles are for lithofacies B.

$$g'_{ac}(x) = \frac{1}{\pi} \operatorname{Re} \left[ \int_0^{\infty} \frac{\hat{R}(k)}{\hat{\psi}_{\sigma}(k)} e^{-ikx} dk \right]. \quad (19)$$

The impedance  $g_{ac}(x)$  is obtained by integrating Eq. (19).

In order to evaluate Eq. (19) for the numerically (hydrodynamically) simulated signals, the Fourier transform of the Mexican hat wavelet,

$$\hat{\psi}_{\sigma}(k) = A_0 \sigma \sqrt{\pi} k^2 e^{-(\sigma k/2)^2}, \quad (20)$$

is used along with the Fourier transform of the simulated reflection response,  $R(x)$ .

To carry out the integration in Eq. (19), a discrete mesh,  $k_n = n\pi/L$ , is used, where the reflection signal differs from zero in the range  $0 < x < L$  and  $n$  are integer numbers. For the reflected signals under consideration,  $L \approx 1000$  m is selected. A cutoff is introduced in the integration at  $k_{\max} = 2\pi/\lambda$ , where  $\lambda \approx \sigma$ . This is needed so that  $k$  modes with little reflected energy are not amplified. This keeps noise from being amplified to a point where it can dominate the reflected signal. This is analogous to the  $j_{\min}$  cutoff applied in the DWT.

It is recognized that this application of the FT deconvolution is not the most sophisticated. Most times a noise factor

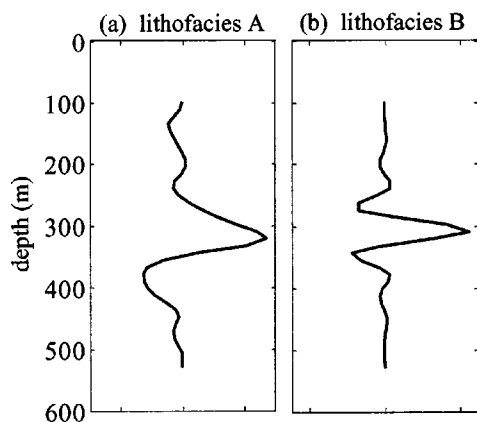


FIG. 11. Wavelets derived from the real seismic data and well log shown as amplitude (arbitrary units) vs depth. (a) Lithofacies A. (b) Lithofacies B.

is used and the spectrum is tapered. It was decided to use this implementation so that a fair comparison can be made to the DWT deconvolution, which is equally unsophisticated. This being said, tests were also done using a more sophisticated FT approach. Although the sidelobe oscillations were reduced, a greater high frequency deconvolution artifact appeared in the main signal.

The results of a deconvolution done with both methods are shown in Figs. 10(a) and 10(b). The signal-to-noise (S/N) ratio for the FT is 13.8 dB compared to 22.1 dB for the DWT. The deconvolution artifacts are also more localized for the DWT. This reduces the interference of multiple stacked packages of reflectors. The DWT is, therefore, the preferred method for the deconvolution.

## V. APPLICATION OF INVERSE MODEL TO REAL SEISMIC DATA

The DWT inverse model is applied to the real seismic data corresponding to the two characteristic cases. First, the incoming wavelets for the two cases are derived. They are estimated by standard wavelet estimation techniques used in many seismic inversions.<sup>17</sup> A section of the seismic data of about a second (1500 m) is used along with the compressional sonic velocity and density well log, corresponding to the seismic data. The derived wavelet, when convolved with the well log reflectivity matches the seismic data to within about 12 dB. Care is taken that the interval corresponding to the characteristic cases does not have a dominant effect on the derivation of the wavelets. The wavelets for the two cases are shown in Fig. 11. Note the differences between them. These differences make the CWT of the reflected signals very difficult to compare to each other and to the well log database because of the imprint of the wavelets on the reflected signal. The two cases have seismic data from two separate seismic surveys, with different acquisition and processing parameters. It is known that the processing was not amplitude preserving. A gas amplitude anomaly, proven by the drill bit, was not seen on these data. It was seen on another dataset that had both superior acquisition and processing. The bandwidth of this dataset was also much better. The DWT inversion of the real reflection seismic is shown in

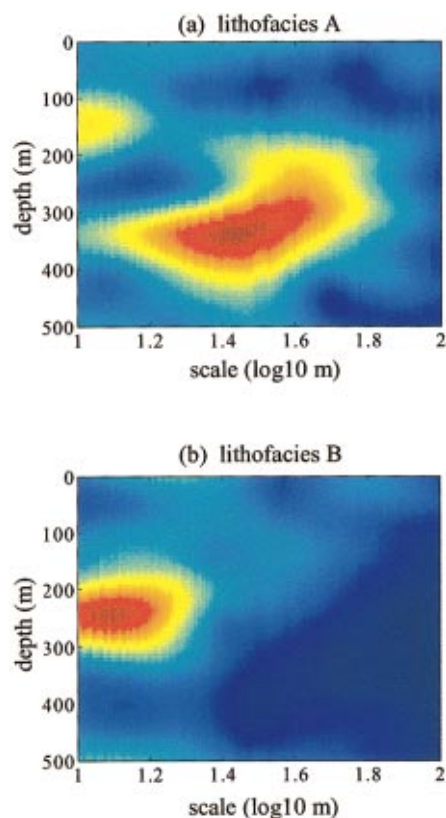


FIG. 12. (Color) CWT of the DWT inversion of the real seismic data. (a) Lithofacies A. (b) Lithofacies B.

Fig. 12. The response is quite similar to the wavelet transform of the well log derivative acoustic impedance (Fig. 1). This is really quite surprising considering the quality of the seismic data. This multiscale character appears to be much more robust to acquisition and processing differences than conventional quantitative interpretation.

## VI. ESTIMATION OF LITHOFACIES PROBABILITY

### A. Calibration using wells

The final component of this project is the collection of a population of well logs, classification of intervals of those well logs according to their lithofacies group, and calculation of the wavelet transforms of the derivatives of the acoustic impedance for the same intervals. After examining the wavelet transforms of each lithofacies population, a suitable parameter of the wavelet transform is chosen which discriminates the lithofacies. The chosen parameter was the log of the average scale, that is bed thickness,  $\langle \sigma \rangle$ . Histograms for each lithofacies are plotted and fit to a Gaussian. The result is shown in Fig. 13. These probability distributions are the conditional probability of the observing a multiscale character in the seismic given that one knows the lithofacies,  $P(\langle \sigma \rangle | \text{lithofacies})$ . There is a reasonable size population for each lithofacies group—11 samples for lithofacies A and 15 samples for lithofacies B. These samples are independent and come from 14 different wells.

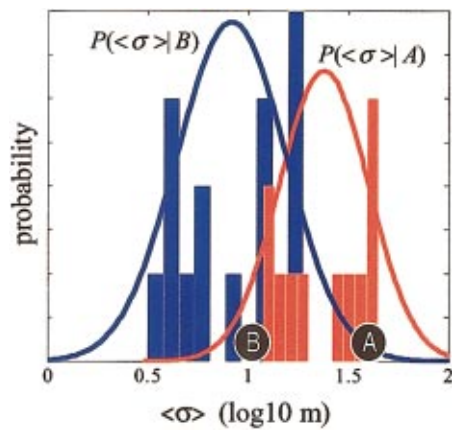


FIG. 13. (Color) Conditional probabilities of scale given the lithofacies. Histograms are the well log distributions, lines are Gaussian distributions fit to the histograms. The conditional probability of lithofacies A is shown in red and lithofacies B is shown in blue. The values of the average scale,  $\langle\sigma\rangle$ , expressed in the CWT of the real seismic data displayed in Fig. 12 are shown as large black circles labeled as (A) lithofacies A and (B) lithofacies B.

## B. Bayesian inversion for lithofacies probability

The issue with using the conditional probabilities,  $P(\langle\sigma\rangle|\text{lithofacies})$ , is that one measures the multiscale character of the seismic,  $\langle\sigma\rangle$ , and wishes to know the probability of a specific lithofacies,  $P(\text{lithofacies}|\langle\sigma\rangle)$ . The conditional probability that we know is in the wrong order. One can use Bayes' Theorem to solve for the desired probability given the known conditional probability.<sup>18</sup> Assuming that the probabilities of the lithofacies are equal before taking into account the multiscale character, the probability of a lithofacies given the multiscale character can be calculated via a Bayesian inversion giving

$$P(A|\langle\sigma\rangle) = \frac{P(\langle\sigma\rangle|A)}{P(\langle\sigma\rangle|A) + P(\langle\sigma\rangle|B)}, \quad (21)$$

and

$$P(B|\langle\sigma\rangle) = \frac{P(\langle\sigma\rangle|B)}{P(\langle\sigma\rangle|A) + P(\langle\sigma\rangle|B)}. \quad (22)$$

For the two characteristic cases, whose inverted seismic reflections CWT are shown in Fig. 12, the logs of the average scale  $\langle\sigma\rangle$  are 1.6 for lithofacies A and 1.0 for lithofacies B. The value for lithofacies A corresponds to the upper part of the package. The lower part of the package has many scales ranging from 1.2 to 1.5. Given the observed multiscale character of the seismic for lithofacies A one would estimate the probability of it being A to be 95%. The certainty of lithofacies B being B, given the multiscale character of its seismic reflection, is not as great. It is 77%. These probabilities are quite useful and can be directly used in making decisions about whether or not to drill wells.

## VII. CONCLUSIONS

Geologic lithofacies are quantitatively identified by the inversion and wavelet decomposition of the seismic reflection. It is robust, working on data where standard, amplitude

based, quantitative interpretation does not work well. This can be done even if the bandwidth of the seismic data is not good enough to resolve the dominant bed thickness of the lithofacies group. The analytic DWT inverse formula for the wavelet transform of the acoustic impedance given the seismic reflection response has been justified by the forward modeling. A linear approximation enables the simple inverse formula and is justified by the insignificance of multiple reflections. The DWT performs better than the FT, having fewer deconvolution tail artifacts. Real seismic data show the response predicted by the forward modeling. When this is combined by the conditional probabilities derived from a population of well logs, the probability of a lithofacies group is reliably estimated.

Further work needs to be done. The performance of the DWT can be improved. The application of this technology is still crude, especially with respect to how it handles noise. More sophisticated approaches need to be implemented and their performance with respect to noise needs to be quantified.

## ACKNOWLEDGMENTS

The authors would like to acknowledge the support of BHP Billiton Petroleum, and the help of Bruce Asher, Gillian Apps, Chris Lerch, and Val Lincecum.

<sup>1</sup>P. J. Talling, *Sedimentology* **48**, 1297 (2001).

<sup>2</sup>D. H. Rothman and J. P. Grotzinger, *SFI Studies in the Science of Complexity* (Addison-Wesley, Reading, MA, 1996), Vol. XXV, p. 117.

<sup>3</sup>C. Chen and R. Hiscott, *J. Sediment. Res.* **69**, 505 (1999).

<sup>4</sup>C. J. Velzeboer, *Geophysics* **46**, 843 (1981).

<sup>5</sup>G. Partyka, J. Gridley, and J. Lopez, *The Leading Edge* **18**, 353 (1999).

<sup>6</sup>S. Mallat, *A Wavelet Tour of Signal Processing* (Academic, New York, 2000).

<sup>7</sup>F. J. Herrmann, Ph.D. thesis, Delft Technical University (1997).

<sup>8</sup>J. R. Jimenez and R. J. Michelena, *Proceedings of the Society of Exploration Geophysicists Annual Meeting*, Houston, TX (1999).

<sup>9</sup>S. Sun, R. Siegfried, and J. Castagna, *Proceedings of the Society of Exploration Geophysicists Annual Meeting*, Salt Lake City, NV (2002), p. 457.

<sup>10</sup>L. D. Landau and E. M. Lifshitz, *Fluid Mechanics* (Pergamon, New York, 1959), Chaps. 1 and 8.

<sup>11</sup>M. Strauss, Y. Kaufman, M. Sapir, P. Amendt, R. A. London, and M. E. Glinsky, *J. Appl. Phys.* **91**, 4720 (2002).

<sup>12</sup>A. N. Akansu and R. A. Haddad, *Multiresolution Signal Decomposition* (Academic, New York, 1992), Chap. 5.

<sup>13</sup>W. H. Press, S. A. Teukolsky, W. T. Vetterling, and B. P. Flannery, *Numerical Recipes*, 2nd ed. (Cambridge University Press, Cambridge, U.K., 1992), Chap. 13.

<sup>14</sup>M. L. Wilkins, Lawrence Livermore National Laboratory Report No. UCRL-ID-113198 (1993).

<sup>15</sup>G. Paltauf and H. Schmidt-Kloiber, *J. Appl. Phys.* **82**, 1525 (1997).

<sup>16</sup>I. Daubechies, *Ten Lectures on Wavelets* (SIAM, Philadelphia, PA, 1992), p. 258.

<sup>17</sup>R. White, R. Simm, and S. Xu, *Geophys. Prospect.* **46**, 323 (1998).

<sup>18</sup>R. T. Clemen, *Making Hard Decisions* (Duxbury, Pacific Grove, CA, 1996), p. 226.